Hybrid adaptive and computational light-sheet fluorescence microscopy

Wilding, Dean; Pozzi, Paolo; Soloviev, Oleg; Vdovin, Gleb; Fiolka, Reto; Verhaegen, Michel

DOI
10.1117/12.2287661

Publication date
2018

Document Version
Final published version

Published in
Proceedings of SPIE

Citation (APA)
Wilding, D., Pozzi, P., Soloviev, O., Vdovin, G., Fiolka, R., & Verhaegen, M. (2018). Hybrid adaptive and computational light-sheet fluorescence microscopy. In T. G. Bifano, J. Kubby, & S. Gigan (Eds.), *Proceedings of SPIE: Adaptive Optics and Wavefront Control for Biological Systems IV* (Vol. 10502). Article 1050212 (Proceedings of SPIE; Vol. 10502). SPIE. https://doi.org/10.1117/12.2287661

Important note
To cite this publication, please use the final published version (if applicable).
Please check the document version above.

PROCEEDINGS OF SPIE

SPIEDigitalLibrary.org/conference-proceedings-of-spie

Hybrid adaptive and computational light-sheet fluorescence microscopy

Dean Wilding, Paolo Pozzi, Oleg Soloviev, Gleb Vdovin, Reto Fiolka, et al.

Dean Wilding, Paolo Pozzi, Oleg Soloviev, Gleb Vdovin, Reto Fiolka, Michel Verhaegen, "Hybrid adaptive and computational light-sheet fluorescence microscopy," Proc. SPIE 10502, Adaptive Optics and Wavefront Control for Biological Systems IV, 1050212 (23 February 2018); doi: 10.1117/12.2287661

SPIE.

Event: SPIE BiOS, 2018, San Francisco, California, United States

Hybrid adaptive and computational light-sheet fluorescence microscopy

Dean Wilding[a], Paolo Pozzi[a], Oleg Soloviev[a,b], Gleb Vdovin[a,b], Reto Fiolka[d], and Michel Verhaegen[a]

[a]Delft Center for Systems and Control, TU Delft, Mekelweg 2, 2628 CD Delft, The Netherlands
[b]Flexible Optical B.V., Polakweg 10-11, 2288 GG Rijswijk, The Netherlands
[c]ITMO University, Kronverksky 49, 197101 St Petersburg, Russian Federation
[d]Department of Cell Biology, University of Texas Southwestern, 6000 Harry Hines Blvd, Dallas TX 75390, U.S.A.

ABSTRACT

The light-sheet fluorescence microscopy is an excellent tool for the investigation of large three dimensional microscopy samples at the cellular level, however, the ability to resolve features is strongly affected by the presence of scattering and aberrations. These effects are two fold in light-sheet microscopy, as the illumination path providing the optical sectioning and the fluorescence detection path are both affected by the aberrations in different ways. To overcome these difficulties, we have developed hybrid adaptive optical and computational microscopy techniques to remove the effect of the aberrations in both the excitation and the fluorescence paths of these microscopes.

Keywords: Adaptive optics, deconvolution, microscopy, light-sheet

1. INTRODUCTION

Light-sheet fluorescence microscopy (LSFM)[1,2] is a type of wide-field microscopy that achieves optical sectioning by orthogonal excitation and detection of fluorescence. It is used for a range of applications, but generally is used to image inside of three-dimensional samples with high spatio-temporal resolution.

The optical inhomogeneity introduced by three-dimensional biological samples leads to phase aberrations implying that the recorded image misrepresents the true fluorophore distribution. This can be corrected either by adaptive optics (AO)[3,4] or through post-processing (PP) tools such as deconvolution.[5] The use of post-processing can only recover information lost through aberrations if it is present in a set of diverse observations, either by acquiring the data from different angles, or by intentional modification of the pupil as explain in the authors previous work.[6,7]

In the presence of these phase aberrations, the excitation profile of the LSFM is distorted and this strongly affects the observed fluorescence independent of what correction done on the detection path. In order to have images that do not misrepresent the fluorophore distribution, one should correct the aberrations in both the excitation and the detection light. In LSFM the correction is commonly attempted through post-processing multiple observations of the fluorescence distribution from multiple angles, a recent example of this approach may be found in Liu et al.[8]

In this article, it is outlined how a joint adaptive correction on the illumination may be combined with a computational correction on the detection light, i.e. post-processing. The rationale behind this approach is that whilst it is possible to employ a three-dimensional correction in post-processing, physical correction of the light-sheet improves greatly the optical sectioning hereby the signal-to-noise ratio (SNR), reduces the amount of out-of-focus fluorescence and thereby, improves any post-processing results. Results from imaging *casper fli:GFP* zebrafish will be shown to highlight the improvement the extra adaptive correction makes.

Adaptive Optics and Wavefront Control for Biological Systems IV, edited by Thomas G. Bifano, Joel Kubby, Sylvain Gigan, Proc. of SPIE Vol. 10502, 1050212 · © 2018 SPIE · CCC code: 1605-7422/18/$18 · doi: 10.1117/12.2287661

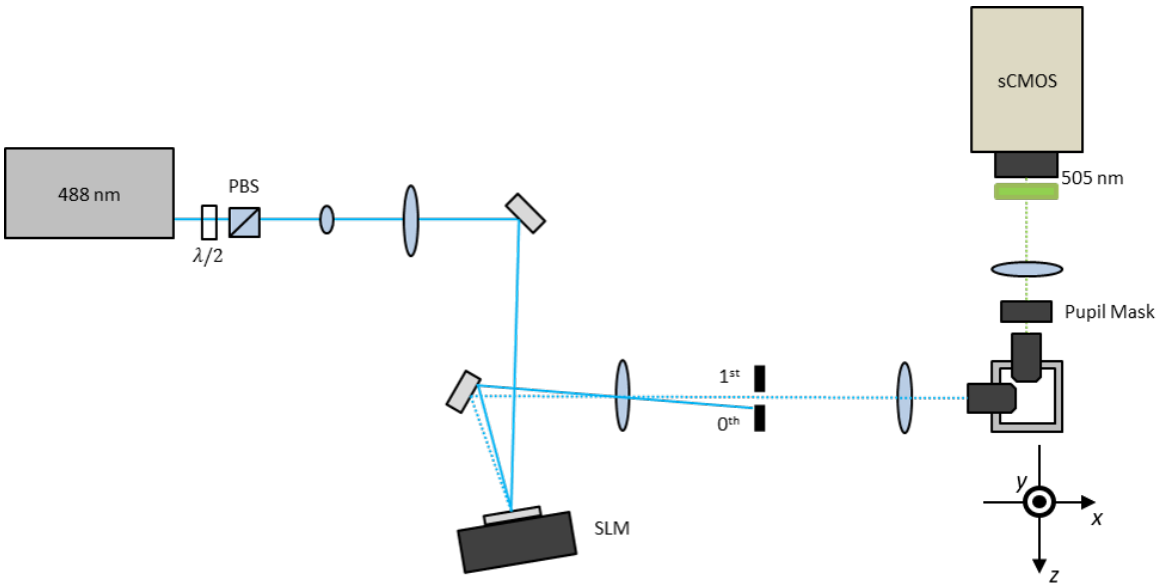

Figure 1. A schematic of the optical system for this hybrid correction scheme: it is a standard LSFM configuration except with the addition of the pupil mask and the SLM in excitation.

2. METHODS

2.1 Experimental Description

The experimental setup used for this work is shown in Fig. 1. It shows two optical paths. One for fluorescence detection that has microscope (NA= 0.5 UMPLFLN 20×W, Olympus, Japan / AC254-200-A-ML, Thorlabs, U.S.) connected to a custom made sample chamber; this is along the direction labelled z. This path also contains an optional pupil mask for modification of the optical transfer function (OTF) of the microscope allowing diversity-based image deconvolution. The second path is for excitation and has a spatial light modulator (SLM) (512×512 HS, Meadowlark Optics, U.S.) conjugated via a telescope (2×AC508-200-A-ML, Thorlabs, U.S.) to the pupil plane of the excitation objective (NA= 0.3 UMPLFLN 10×W, Olympus, Japan); this is along the direction labelled x. This excitation configuration allows for phase modulation in the pupil plane and the generation of a light-sheet by cancellation of the focusing power of the objective in the vertical direction y.

The samples used are *casper fli:GFP* zebrafish 5 days post-fertilisation (dpf) fixed in para-formaldehyde and mounted in square 1 × 1mm capillary tubes (Vitrotubes^{TM}, VitroCom, U.S.), these are secured using a 0.5% agarose gel. The capillaries are aligned with the optical axes and three-dimensional acquisition is done by moving the sample with a stepper motor stage along z (USB 4D Stage, Picard Industries, U.S.) with minimum step size $\Delta z = 1.5\mu$m. The acquired frames are registered using two-dimensional Fourier Cross-Correlation (FCC) to adjust for any sample drift between frames. The same generalised procedure is done in three-dimensions to ensure the overlap of the multiple image stacks for post-processing.

2.2 Sensor-less Optimisation for Light-Sheet Microscopy

In the author's previous work, a wavefront sensor was successfully introduced in the imaging path to correct for aberrations in the excitation.[4] Whilst this approach worked, it could only be used on limited areas of the field-of-view due to its need of a "guide star" area of fluorescence in the centre of the field-of-view. To overcome this a sensor-less approach has been developed for the optimisation of the fluorescence signal. Finding a sensor-less metric has proven itself a difficult problem, since many metrics that can be defined for illumination optimisation in LSFM will lead to changes in imaging plane or concentration of the beam in sharper or brighter regions of the sample. To avoid this an approach based on introducing *a priori* information has been employed.

Further author information: (Send correspondence to D.W.)
D.W.: E-mail: d.wilding@tudelft.nl, Telephone: +31 15 278 1758

Sensor-less optimisation of the excitation light is done by generating a periodic array of spots in the sample using the Gerchberg-Saxton algorithm.[9] This gives the phase pattern ϕ_a for the SLM that will generate a structured illumination pattern (SIM) along the LS plane. In the focal region of the LS, therefore, one expects to have a peak in the Fourier spectrum of the line profile, $l(y)$, through the focus at a given spatial frequency given by the designed array spacing (ν_a). Despite the arbitrary spacing of fluorophores in most samples, the introduced structured illumination frequency will nearly always provide a signal for optimisation on an extended fluorophore distribution. This will still limit the areas that can be used for the optimisation procedure, but it is more general and simpler than the wavefront sensor approach.

The phase in the pupil for the optimisation, φ, is given by the summation of Zernike polynomials $\{\mathcal{Z}_n\}$ with a set of coefficients $\boldsymbol{\alpha} = \{\alpha_1 \dots \alpha_N\}$ and the array phase ϕ_a:

$$\varphi = \phi_a + \sum_{n=1}^{N} \alpha_n \mathcal{Z}_n, \tag{1}$$

where n is the Noll index up to an arbitrary number of polynomial functions N. Mainly here, one is concerned with the low-order aberration modes that effect the LS more significantly and therefore, $N = 10$ is chosen to limit the optimisation time and photo-bleaching effects. The resultant image, $i(x, y, z)$ given by these modes, $\boldsymbol{\alpha}$, applied to the SLM may be modelled as the following equation if the focal position is at $(x = y = z = 0)$:

$$i(x, y, \boldsymbol{\alpha}) = \left[h_{\text{det}}(x, y, z) * (o(x, y, z) \times h_{\text{ex}}(x, y, z, \boldsymbol{\alpha}))\right]_{z=0}. \tag{2}$$

where h_{det} and h_{ex} are the detection and excitation point-spread functions respectively. $*$ is the convolution operator and $\times$ the point-wise multiplication of the functions. The spectrum of line profile $\mathcal{L}(\nu, \boldsymbol{\alpha})$ can then be calculated by:

$$\begin{aligned} l(y, \boldsymbol{\alpha}) &= \sum_{x=-\delta/2}^{x=\delta/2} i(x, y, \boldsymbol{\alpha}), \\ \mathcal{L}(\nu, \boldsymbol{\alpha}) &= \mathcal{F}\left\{l(y, \boldsymbol{\alpha})\right\}, \end{aligned} \tag{3}$$

where $\mathcal{F}$ denotes the discrete 1D Fourier transform over the line and δ is the depth-of-focus of the excitation objective to increase the signal-to-noise ratio. With the above model, the optimisation problem to remove the aberrations in the excitation path has the following mathematical form:

$$\max_{\boldsymbol{\alpha}} \frac{\sum_{\nu=-\nu_a-\Delta\nu/2}^{\nu=-\nu_a+\Delta\nu/2} \mathcal{L}(\nu, \boldsymbol{\alpha}) + \sum_{\nu=\nu_a-\Delta\nu/2}^{\nu=\nu_a+\Delta\nu/2} \mathcal{L}(\nu, \boldsymbol{\alpha})}{\sum_{\nu} \mathcal{L}(\nu, \boldsymbol{\alpha})}, \tag{4}$$

where ν_a is the spatial frequency of the focal SI pattern, $\Delta\nu$ is the bandwidth of the peak and the division is essentially a normalisation to account for the photo-bleaching of the sample. This function may be optimised with a suitable optimisation algorithm, and it was found that a coordinate search (CS) is of sufficient complexity, however, more advanced algorithms could be used. The optimisation procedure for the results in Section 3 required 100 iterations to correct $N = 10$ modes, this is a high number because the samples where degraded when imaged and the signal-to-noise ratio (SNR) was poor and extra frames helped to converge to a maximum.

The sensor-less optimisation procedure was done before any imaging took place so that the loss of SNR would not be unfairly biased towards the data acquired pre-optimisation. The next step after optimisation was to acquire a dataset without any pupil modification, after which a number D of datasets of the same region-of-interest were imaged without the AO correction and then with the AO correction; *i.e.* $D + 1$ acquisitions in total. Despite attempting to make comparison at the same SNR, due to this acquisition procedure the AO datasets are acquired with a lower SNR due to the loss of fluorescence due to photo-bleaching during the previous acquisitions.

2.3 Data Post-Processing

The post-processing in this paper is a blind deconvolution approach that relies on intentionally introduced diversity. It has been shown that possible to reproducibly extract both the aberration kernel and the estimated object from a set of diverse observations.[6,10] Specifically, when considering light-sheet microscopy the required diversity can arise from various sources: different views of the three-dimensional object introducing phase and amplitude diversity or from one of these alone introduced intentionally in the optical path.

In the light-sheet experimental setup used, square capillaries are employed and these do not allow for arbitrary rotation of the sample (other than to the 4 orthogonal directions). In this case, it is possible instead to use a mask in the aperture to create different observations. By blocking a part of the aperture, one changes the PSF/OTF and therefore, it moves the zeros in the OTF spectrum produced by the presence of aberrations.

The regular method in LSFM is to do a full three-dimensional deconvolution, however, in this case the axial correction will be done using physical AO and therefore, it can be processed xy plane by xy plane. The aberration will vary plane-to-plane since the fluorescence must travel through an increasingly thick layer of tissue before reaching the objective.

3. IMAGING RESULTS

3.1 Sensor-less Adaptive Optics

A comparison between the slices acquired with and without the AO correction can be found in Fig. 2, and it can be observed that using the AO there is recovery of axial information that has been lost in the imaging process. It does appear from these frames that the correction does not make the image uniformly better in three-dimensions. This is to be expected, the AO correction found by the algorithm will be the average best correction over the whole field-of-view in the central z plane that was used to compute the metric. The further away from this plane, the more ill-suited the correction will be to the aberration in this location. This effect is known as anisoplanatism.

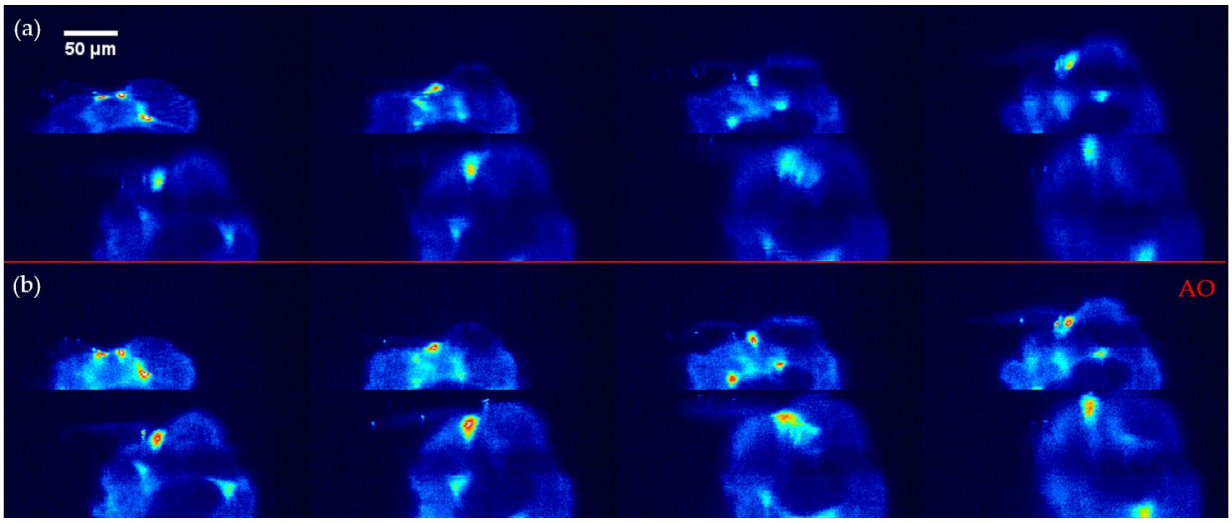

Figure 2. (a) xz slices through a unprocessed LSFM dataset showing a sections of *casper fli:GFP* zebrafish tail. (b) The same region imaged after a sensor-less optimisation procedure.

3.2 Adding Post-Processing

To correct the aberrations in the detection it is necessary to process this data, as discussed in Section 2 plane-by-plane. The chosen orientation is the xy plane to allow the aberrations to vary as one goes deeper into the sample. Two parts of the sample were imaged, the tail, which is less likely to suffer from aberrations and scattering and the body of larva that has much more scattering and aberrations.

Firstly, in Fig. 3, maximum intensity projections (MIPs) of the tip of tail is shown without post-processing (PP), with only PP and then with both PP and AO. The result here is most obvious in the axial projection, where the AO has been used. The dataset without the AO correction shows that some areas have been heavily distorted by the aberrations and are corrected in the optimised version.

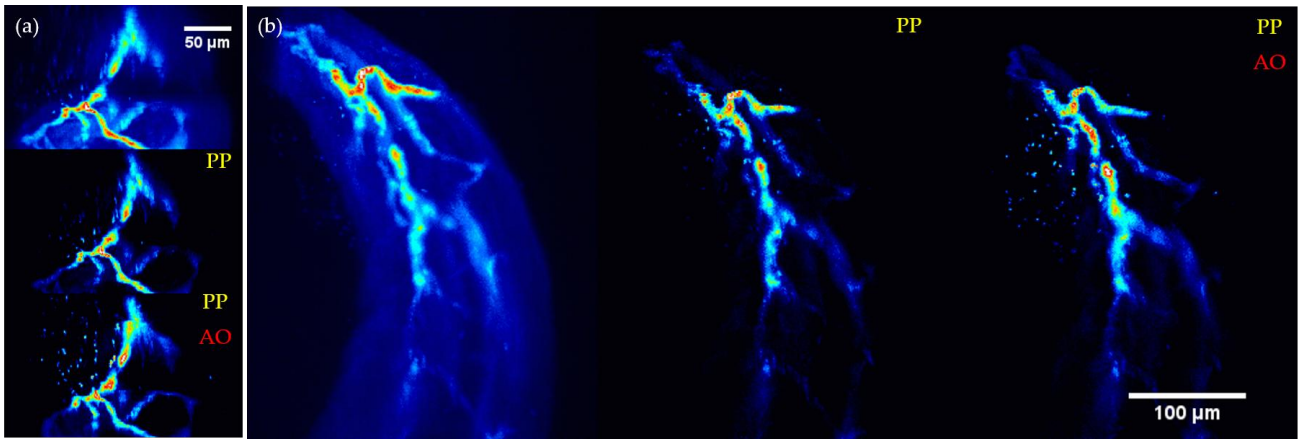

Figure 3. MIPs of a *casper fli:GFP* zebrafish tail with and without AO correction in excitation and or PP in detection. (a) xz maximum intensity projection. (b) xy maximum intensity projection.

Both methods can be repeated on other areas of the sample, this time in the body of the fish larva where there is a greater scattering, which makes PP more challenging. In Fig 4 the results from the same process can be seen. One of the biggest difference between the dataset in Fig 3 and Fig 4 is the extra scattering. The scattering produces a background that is reduced by the PP methodology, but not completely removed and the AO (data not shown) also reduces this background as there is less out-of-focus fluorescence with a thinner light-sheet. The scattering comes from two sources, scattered illumination light that excites out-of-plane fluorophores and also from directly scattered fluorescence from in-plane fluorophores. AO in excitation is able to dampen the former, but can do nothing for the latter.

4. DISCUSSION

The results show that the optimisation of the fluorescence signal with a structured illumination pattern can correct for aberrations in a three-dimensional sample. This correction, based on the optical and optimisation scheme that was used is isoplanatic in its nature. This means that it is one average correction for the entire field-of-view. In microscopy in general, the correction required is not isoplanatic and one corrective phase cannot improve the quality of the image over the whole field-of-view.

Optimisation specifically has the effect of improving the average signal over the field-of-view. In the case of the SI pattern, if it possible to improve the top part of the signal greater than the reduction in the bottom part of the sheet then the algorithm could converge to this solution. This appears in part to be the case in Fig.3, where the top part of the image is improved and the left-bottom quarter appears to be worse. This effect arises from anisoplanatism and could be corrected by computing a correct for each area of the SI pattern applied for optimisation. This could take more time to isolate the aberration for each region of the sample, but would yield a better final result.

In Fig 5 a comparison between using PP to correct for the axial aberration and using a combination of AO and PP is shown. The deconvolution here is applied in the xz plane rather than xy, therefore, correcting for the three-dimensional PSF as it varies along the beam path. Here it is demonstrated that using PP alone on the data to correct for aberrations introduced by the excitation is not an optimal solution. The addition of the physical aberration correction provides an increase in the optical sectioning ability of the microscope and thus improves the image quality compared with deconvolution alone.

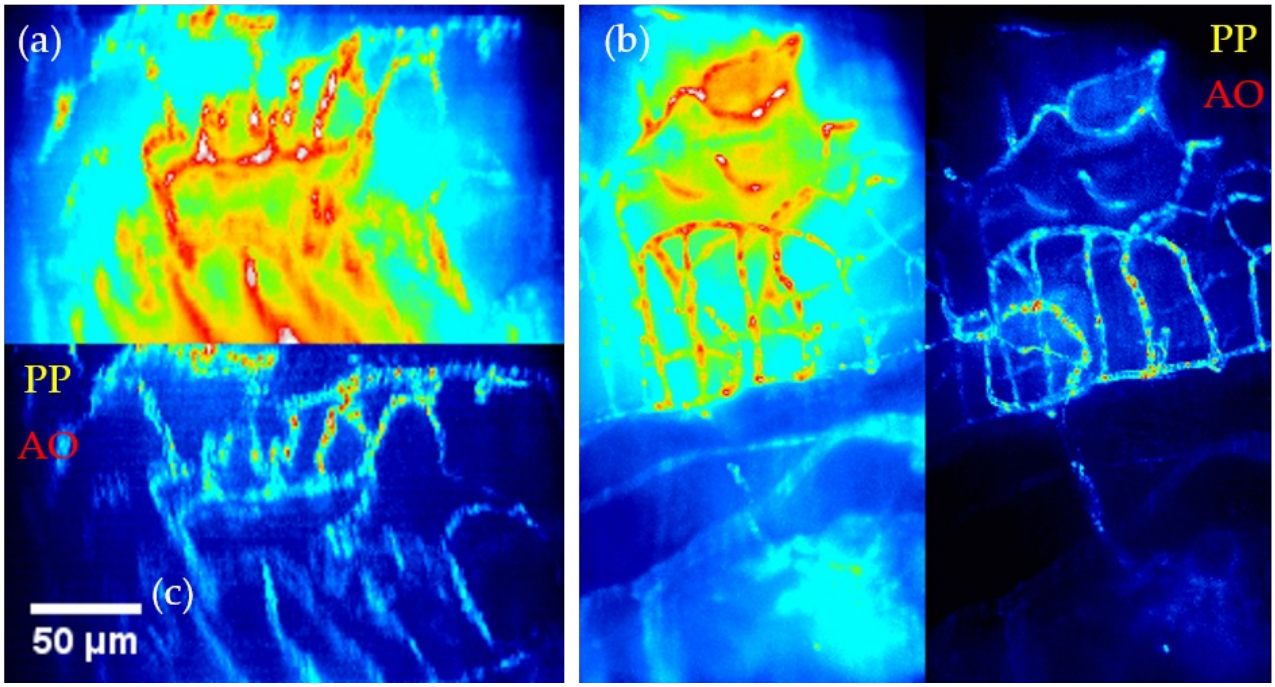

Figure 4. MIPs of a *casper fli:GFP* zebrafish body with and without adaptive optics (AO) correction in excitation. (a) xz maximum intensity projection. (b) xy maximum intensity projection.

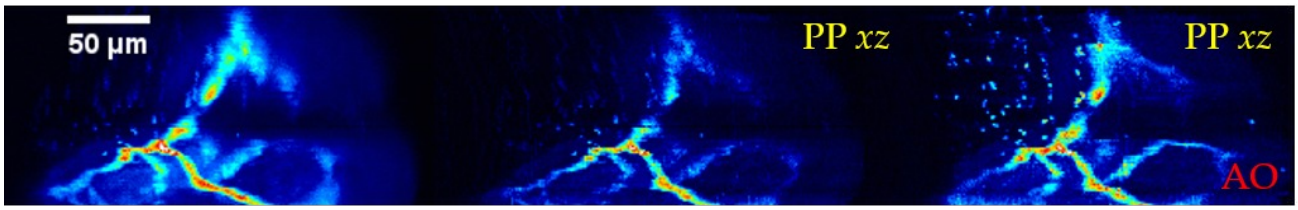

Figure 5. xz projections through a zebrafish sample. A comparison between using PP alone to remove aberrations and using a combination of AO and PP. The left most image shows the unprocessed LSFM data without AO.

From this comparison, it is clear that the physical correction has a greater corrective power than simply using PP alone. Here is the difficulty with using only PP to correct for aberrations: one can never be sure that the result given is the true fluorophore distribution. In contrast, with the optimisation of the SI pattern from physical principles one can be certain that if the signal is maximised that the aberrations have been removed, giving extra confidence in the results given by the PP algorithms that still able to correct for effects beyond the range of current AO techniques.

To conclude, it has been shown in this paper that the addition of physical adaptive optics correction in the excitation of a light-sheet microscope can improve the three-dimensional images that the microscope produces when compared with PP alone. The AO correction gives different results than PP and highlights the misrepresentation of the fluorescence distribution that phase aberrations introduce in large biological samples such as zebrafish embryos.

ACKNOWLEDGMENTS

The authors would like to acknowledge the technical contributions of W.J.M. van Geest and C.J. Slinkman; M.J.M. Schaaf and A.H. Meijer from Leiden University for zebrafish samples along with support from E.C.M Carroll at TU Delft. The research leading to these results has received funding from the European Research

Council under the European Union's Seventh Framework Programme (FP7/2007-2013). ERC Grant Agreement No. 339681.

REFERENCES

[1] Voie, A., Burns, D., and Spelman, F., "Orthogonal-plane fluorescence optical sectioning: Three-dimensional imaging of macroscopic biological specimens," *Journal of microscopy* **170**(3), 229–236 (1993).

[2] Huisken, J., Swoger, J., Del Bene, F., Wittbrodt, J., and Stelzer, E. H., "Optical sectioning deep inside live embryos by selective plane illumination microscopy," *Science* **305**(5686), 1007–1009 (2004).

[3] Bourgenot, C., Saunter, C. D., Taylor, J. M., Girkin, J. M., and Love, G. D., "3d adaptive optics in a light sheet microscope," *Optics express* **20**(12), 13252–13261 (2012).

[4] Wilding, D., Pozzi, P., Soloviev, O., Vdovin, G., and Verhaegen, M., "Adaptive illumination based on direct wavefront sensing in a light-sheet fluorescence microscope," *Optics express* **24**(22), 24896–24906 (2016).

[5] Swoger, J., Verveer, P., Greger, K., Huisken, J., and Stelzer, E. H., "Multi-view image fusion improves resolution in three-dimensional microscopy," *Optics express* **15**(13), 8029–8042 (2007).

[6] Wilding, D., Soloviev, O., Pozzi, P., Vdovin, G., and Verhaegen, M., "Blind multi-frame deconvolution by tangential iterative projections (tip)," *Opt. Express* **25**, 32305–32322 (Dec 2017).

[7] Wilding, D., Pozzi, P., et al., "Phase diversity based object estimation in light-sheet fluorescence microscopy," in [*Bio-Optics: Design and Application*], BoTu2A–2, Optical Society of America (2017).

[8] Liu, S., Nie, J., Li, Y., Yu, T., Zhu, D., and Fei, P., "Three-dimensional, isotropic imaging of mouse brain using multi-view deconvolution light sheet microscopy," *Journal of Innovative Optical Health Sciences* **10**(05), 1743006 (2017).

[9] Gerchberg, R. W. and Saxton, W. O., "A practical algorithm for the determination of phase from image and diffraction plane pictures," *Optik* **35**, 237246 (1972).

[10] Yaroslavsky, L. P. and Caulfield, H. J., "Deconvolution of multiple images of the same object," *Applied Optics* **33**, 2157 (apr 1994).